

Characterization of aluminium matrix composite of Al-ZnSiFeCuMg alloy reinforced with silica sand tailings particles

Sukanto¹, Rudy Soenoko², Wahyono Suprpto², Yudy Surya Irawan²

¹ Politeknik Manufaktur Negeri Bangka Belitung, Kawasan Industri Airkantung, Sungailiat, Bangka, 33211, Indonesia
Phone: (+62) 717-93586, Fax: (+62) 717- 93585

² Fakultas Teknik, Universitas Brawijaya, Jl. M.T. Haryono 167, Malang, Indonesia

ABSTRACT – Due to the increased demand for aluminium and the prohibitive cost of producing primary aluminium, the process of making AMCs using recycled aluminium alloy as a matrix and silica sand tailing without leaching as a filler is essential to be developed. For more cost-effective, the purpose of this study is to make particulate aluminium composite matrix AMCs with a matrix of recycled aluminium and reinforced with silica sand tailing without leaching. This research involves the effect of differences in grain size and filler weight percentage on matrix Al-ZnSiFeCuMg recycled aluminium alloy powder. This study used powder metallurgy technology as well as two-way hot-compaction (300°C) and applied a sintering temperature of 550°C. Density, hardness, and wear testing, as well as microstructure analysis, were conducted to determine the characteristics of the resulting AMCs. An increase in hardness of 67% was achieved by the AMCs-164 μm -20%SiO₂ specimen, which used a filler grain size of 164 μm wt.20%. Meanwhile, AMCs-31 μm -20%SiO₂, which used a filler grain size of 31 μm , only increased by 63%. The wear test result also showed a lower wear rate achieved by the AMCs-164 μm -20%SiO₂ specimen. The results analyses using SEM-EDS instruments showed higher agglomeration and porosity in specimens using a filler grain size of 31 μm , while AMCs using a filler grain size of 164 μm showed an even spread of filler powder. Therefore, AMCs that used 164 μm powder-sized fillers have a stronger bond between the filler and the matrix and produce AMCs that are harder than AMCs that use 31 μm fillers.

ARTICLE HISTORY

Revised: 24th Jan 2020

Accepted: 20th Mar 2020

KEYWORDS

Silica-sand-tailing;
aluminium matrix composite;
grain size;
hot compaction;
sintering;
hardness;
wear resistance

INTRODUCTION

Particulate-Reinforced Aluminium Matrix Composite (AMCs) materials are lightweight. They have high specific strength, hardness, fatigue resistance, and excellent wear resistance, making them very attractive to be applied in the aerospace, automotive, and military industries [1]. Besides, the advantage of AMCs materials is that the types of their materials (matrix and filler), as well as their processes, may be engineered, which results in composites with specific expected abilities and properties [2]. Aluminium is the most economical metal as a matrix because it can provide a weight reduction of up to 60% compared to an iron metal matrix. Also, automotive component design can be developed to produce a longer product life [3]. Several studies on AMCs reinforced by ceramic materials such as SiC, C, Al₂O₃, SiO₂, B, BN, B₄C, AlN and others have recently been carried out [4]. One of the aims of the study was to find a replacement material for friction brakes that is free from asbestos or Non-Asbestos (NOB) [5, 6]. Asbestos-based material is hazardous for the health of lungs, and thus most countries in the world have banned it is the production and use [7].

Research on AMCs reinforced by 25% silicon carbide showed that hardness could be increased by 150% from 30 HRB to 75 HRB, but fragility also increased by up to 33% [8]. Meanwhile, Agbeleye et al.[9], who examined AMCs with a wt.15% clay filler, found an increase in hardness by 78%, from 43 HV to 76.7 HV. Clay material is hard because it contains a chemical composition of 45% SiO₂ and 33.74% Al₂O₃. Therefore, some AMCs have been made using a type of filler material containing SiO₂ compounds such as silica sand, rice husk ash, and others. This is considering that SiO₂ compounds have the advantage of being relatively hard and light and thus are often used as filler powder reinforcement in the manufacture of composites or as coatings [10, 11]. The aim of their overall research is to be applied as a replacement material for Asbestos-based friction brakes. The processing efficiency of aluminium metal recycling reaches 95% compared to primary aluminium processing. This situation has spurred the increase of recycled aluminium production in Europe, reaching up to 53% of total European aluminium production in 2017 [12,13]. China in recent years should devote greater attention to build an efficient recycled aluminium system to ensure a sustainable supply for the increased global demand for aluminium metal. Therefore, the optimization of using recycled aluminium metal alloy as the basic material for making AMCs is very important [14]. Sand waste in the form of fine soil remnants from the grinding and extracting of tin on the Bangka and Belitung islands, called tailings, has occupied an area of approximately 64,255 Ha of the total area of the former tin mine covering 125,875 Ha [15]. These economic values of silica sand tailings can be increased if they are made into nano-silica material by grinding using a crusher and ball mill, to reduce the size to 200 mesh or 74 μm

[16]. Silica sand or quartz sand from Bangka Belitung is well known to have the best quality in Indonesia [17]. According to research by Wahyudi and Amalia [18], silica sand leaching can produce chemical products with compositions of 98.75% SiO₂, 0.079% TiO₂, 0.054% Al₂O₃, 0.389% Fe₂O₃ and 0.25% LOI. However, the leaching process to obtain relatively high levels of silicon dioxide or quartz has very expensive costs [19, 20].

The process of making composites with the powder metallurgy technology has seven stages: providing powder and additive, blending and mixing, compaction, lubricant removal, sintering, process finishing, and product finishing [21]. Smaller grain sizes will increase the agglomeration property of the powder. Therefore, a good mixing process is needed that can produce a matrix and filler powder mixture with even homogeneity and a low level of filler agglomeration before the mixture is compacted. To avoid agglomeration, the mechanical alloying is often used in the process of mixing the matrix and the filler powders before being compacted [22, 23]. There are several advantages of powder metallurgy compared to other processing technologies: it is economical because it can produce precise products with a high efficiency of material usage (a minimum of 96% will lead to finished products), it is capable to be used for small or tiny products, it is capable of producing finished products or semi-finished products, product dimensions are more accurate than other methods, products can be controlled and deviations are relatively small, and the process can be done at low temperatures. However, the drawback is that during the powder metallurgy process, segregation and agglomeration must be avoided, which can cause uneven and non-homogeneous powder distribution between matrix and filler [22, 23].

Kumar et al. [24] researched AMC's strengthened by three variations of fly ash grain size (50-75 μm , 75-103 μm and 103-150 μm), whereas Gopal et al. [25] researched the effect of weight fraction and particle grain size (10 μm , 30 μm , and 50 μm) of CRT glass for tribology behaviour. Both delivered the same conclusion that the usage of greater grain sizes increased hardness. Jo et al. [26] examined the effect of SiC particle size (1 μm , 7 μm and 20 μm) on the mechanical properties of the resulting hybrid metal matrix composites, and the result was that composites with SiC filler of larger particle sizes had greater wear resistance compared to smaller-sized fillers. Likewise, Chen et al. [27] examined composites using coarser TiC filler particles (2 μm and 20 μm) too, and the results showed greater effects of hardening than composites with smooth TiC particles. All the conclusions of the research are in contrast with the theory regarding the strengthening mechanism of reduced particle diameter sizes and dispersion strengthening [28]. However, the theoretical assumptions apply if small reinforcing particles can be distributed evenly in the matrix or there is a relatively homogeneous mixture of the filler and the matrix. This condition did not occur in some of these studies; instead, the converse condition occurred, with clumping among filler particles that fill packets in the intergranular region.

Chaubey et al. [29] examined the impact of Mg filler of 7.4% grain size on produced AMC's. There were four variations of Mg particle sizes: 0-20 μm , 20-40 μm , 40-80 μm , and 80-100 μm . The research concludes that smaller filler particle sizes led to greater tensile strength from 195 MPa to 295 MPa, increased ductility from 3% to 4%, and a direct increase of the wear rate toward the increase of coarse filler size. This is in line with the theory of particle size reduction strengthening and dispersion reinforcement related to the Hall-Petch relationship [30]. In principle, dispersion strengthening refers to the theory that smaller powder diameters lead to greater contact surfaces and shorter distances among particles, and therefore increased interface bonds when powder metallurgy is carried out, which finally leads to increased mechanical properties of composites [31, 32].

The production of AMC's reinforced with silica sand or SiO₂ powder using the powder metallurgy technique has been carried out by many researchers, where the results showed an increase in mechanical properties through an increase of filler wt.% to a certain percentage, between wt.5% to wt.40% SiO₂. Rizkalla et al. [33] investigated AMC's using filler wt.20% SiO₂ produced AMC's with 34 VHN. Zuhailawati et al. [34] investigated AMC's using filler wt.30% SiO₂ produced AMC's with 230 HV. [20%=150 HV]. Furthermore, Mohan et al. [35] researched AMC's with wt.10% SiO₂ produced AMC's 52 HV. Meanwhile, Aigbodion et al. [6] examined AMC's using asbestos-based commercial brake pad materials produced AMC's with a hardness Of 101 HB. However, these studies still used matrix and filler materials with high chemical composition levels that are greater than 97%. They use commercial aluminium, not aluminium recycled as a matrix and commercial silica as well or leached silica for filler. Yet, the cost of leaching to obtain SiO₂ of high purity levels and the cost of processing primary aluminium are still very expensive [19, 20]. Based on these conditions, the purpose of this study is to increase the direct utilization of silica sand tailings, without being preceded by a leaching process as a filler material and using a matrix made from recycled aluminium alloy. A further goal of this research is to produce AMC's from aluminium recycled reinforced Silica Sand Tailings with certain properties (density, hardness and wear rate), which are expected to be applied as a substitute for asbestos material friction brakes.

METHODS AND MATERIALS

Research Methods

This research on AMC's reinforced by silica sand tailings was carried out using the powder metallurgy technique following the steps of the process as shown in Figure 1, referring to the stages of powder metallurgy [21]. The powder material for the matrix is produced and prepared using the recycling method from automotive component waste and beverage can package waste. The process of melting waste material uses an electric induction furnace at 700-800 °C, and the liquid material is poured into a billet-shaped mould [36]. Afterwards, the billet products are machined by lathe and chips is crushed using a ball mill machine, and the next process is aluminium powder is sieved (mesh). The initial process of powder metallurgy is the silica tailings powder, and Al-ZnSiFeCuMg recycled aluminium alloy powder was prepared in a preheating process at a temperature of 50-60 °C for 30 minutes before the mixing process. The silica filler grain size

variable included $31\ \mu\text{m}$ and $164\ \mu\text{m}$. The wt.% filler variable included 0%, 5%, 10%, 15%, 20%, 25%, and 30%. The mixing of matrix and filler refers to wt.%, with the mixture weight total being 25 grams for one specimen. The process of mixing the powders utilized spiral rods gripped by a drilling machine and rotated at a speed of 200 rpm for 10 minutes.

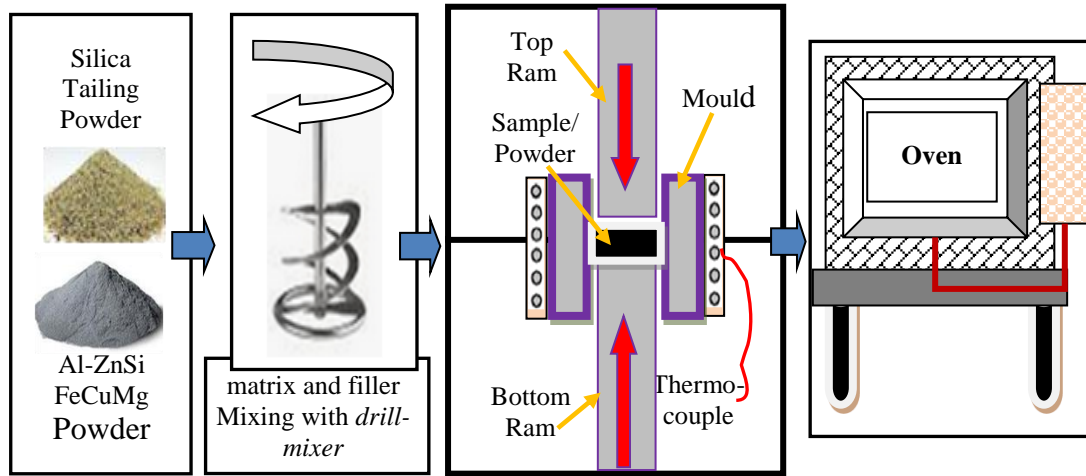


Figure 1. Schematic of the AMCs production process using the technique of powder metallurgy

The moulding for the specimens is ring-shaped, with the dimensions of samples were the large diameter (D) being 40 mm, the small diameter (d) being 17 mm and thickness 8 mm. The 25 gr of mixed powder was placed in the moulding, which had been given a lubricant and then heated using a thermocouple. The compaction process was carried out after the heating temperature reached $300\ ^\circ\text{C}$ with a compaction pressure of 100 MPa for 10 minutes [21]. The compaction process used a two-way hydraulic pump, which consists of a top ram and a bottom ram [37]. After the powder became a solid specimen, the specimen was then removed from the mould, and the lubricant was removed. The average thickness of the produced specimens is in the range of 9-10 mm. In the next process, the specimens were sintered using an electric oven at a temperature of $550\ ^\circ\text{C}$ for 15 minutes.

Characterization of AMCs specimens was carried out through density testing, hardness testing, wear testing, and specimen microstructure analysis. Calculation of the theoretical density of the matrix and filler powder mixture for AMCs was carried out using the following equation [38]:

$$\rho_T = \frac{\sum \%u_i \cdot \rho_{u_i}}{100} = \frac{\%u_1 \cdot \rho_{u1} + \%u_2 \cdot \rho_{u2} + \dots + \%u_n \cdot \rho_{un}}{100} \quad (1)$$

where the variables of $\%u$ and ρ_u are percentages of chemical elements and their densities, while ρ_T is the theoretical density value. Measurement of the density value was performed by using pycnometry, making use of Archimedes' principle (ASTM Standard B962-15), before and after the sintering process [39]. The initial step of measuring the density of the produced AMCs specimens (ρ_{AMCs}) involved the weighing of specimens, which included the scale weight in air (W_a), the weight of a specimen and the specimen basket in water (W_{sb}), the weight of the basket in water (W_b) and the weight of specimen in water ($W_c = W_{sb} - W_b$). If ρ_w is the density of water, then the value of the density of a composite specimen is obtained by calculation using Eq. (2) below [40]. Next, the per cent of porosity $P(\%)$, of hot-compaction AMCs and sintered AMCs were determined using Eq. (3) below:

$$\rho_{AMCs} = \frac{W_a}{W_a - W_c} = \frac{W_a}{W_a - (W_{sb} - W_b)} \times \rho_w \quad (2)$$

$$P(\%) = \frac{\rho_T - \rho_{AMCs}}{\rho_T} \times 100 \quad (3)$$

Hardness testing utilized Hardness Rockwell B [HRB]. In principle, Rockwell hardness is measured based on the depth of an imprint. The utilized hardness testing machine was the Emcotest type N3 HRB hardness testing machine at the Vocational Education Development Center (VEDC) in Malang, Indonesia. The diameter of the utilized steel ball indenter is 1/16" with an initial load of 10 kg and a final load of 100 kg for 10 seconds [8]. Hardness testing with a steel ball indenter is recommended for heterogeneous materials [35].

Wear testing utilized the pin-on-disk wear testing method, which is a simple and often-used method, ASTM: G99-05 standards [41]. The friction force from a revolving disk is applied to a specimen, with the constant shear speed of $0.54\ \text{ms}^{-1}$, a roll diameter of 28 mm, and a roll thickness of 3 mm [42]. The given load was 78.4 N and the wear friction test time was 2 minutes. The roller material is a type of hardened steel alloy with a hardness of 25 HRC and with roughness (R_a) = $4.57\ \mu\text{m}$. The wear rate (W_w) is calculated by Eq. (4) below [43]:

$$W_w = \frac{\Delta W}{2\pi r \cdot n \cdot t} = \frac{m_1 - m_2}{2\pi r \cdot n \cdot t} \quad (4)$$

where m_1 and m_2 are the masses of the specimen before and after the wear test was carried out, ΔW is weight loss, n is revolution per minute, r is the radius of AMCs composite disc, and t is time.

The material powder characterization process utilized several instruments. Sieving used the Retsch Analysensieb sieve shaker machine at the Metal Casting Laboratory of Mechanical Engineering, Brawijaya University. Testing of aluminium alloy composition used the Spectro Spark Analyzer machine, Spectrolab-AMETEK, by the Al-01 method with the SS-6063 standard. The test was conducted at PT. HP. Metal Indonesia, located in Ngoro Industri Persada in East Java, Indonesia. Measurement of grain size distribution utilized the Cilas 1090 Dry Laser Particle Size Analyzer (PSA) machine at the Chemical Engineering laboratory of Brawijaya University. Testing of the chemical composition of silica sand tailings utilized the X'Pert Pro type PanAnalytical X-Ray Diffraction (XRD) machine at the Central Laboratory of the State University of Malang. Microstructure analysis was performed to support the conclusions of this study. The instruments used in microstructure analysis included the Scanning Electron Microscope (SEM) of FEI Quanta FEG 650, FE-SEM type, using the X-act Oxford Instrument EDS detector, at the Central Laboratory of Living Sciences, Brawijaya University (LSIH-UB).

Materials

The AMCs were made using the primary material of Al-ZnSiFeCuMg aluminium alloy powder that resulted from the recycling of aluminium waste produced by $\alpha\beta\gamma$ workshop in Landungsari, Malang, Indonesia. The chemical composition of the Al-ZnSiFeCuMg aluminium alloy, obtained from the Spectro Spark Analyzer test, is shown in Table 1. The test of grain size distribution utilized the Particle Size Analyzer (PSA) instrument with the dry method. It referred to the cumulative grain size distribution values of 10%, 50%, and 90%, denoted as D10, D50, and D90. In this paper, only the grain size distribution of 50% or D50 is recorded. The grain size of the Al-ZnSiFeCuMg aluminium alloy used for the matrix is of D50: $204 \pm 3.81 \mu\text{m}$. The size is the average value of three repeated measurements at $199.88 \mu\text{m}$, $207.31 \mu\text{m}$, and $205.08 \mu\text{m}$, as in Figure 2(a).

Table 1. Chemical composition of Al-ZnSiFeCuMg

Element	Al	Zn	Si	Fe	Cu	Mg	Sn	Pb	Sb	Ni	Other
[%]	83.15	6.16	4.35	2.20	1.30	1.13	0.37	0.33	0.28	0.16	0.56 ¹⁾
STDEV ²⁾	1.33	1.07	0.35	0.20	0.09	0.08	0.04	0.01	0.03	0.02	0

¹⁾ Cr/Mn/Ti/Zr/Ca/Bi/Na/P/Sr/Be/Cd

²⁾ STDEV = Standard Deviation

Table 2. Chemical composition of silica sand tailings

No.	Compound	Formula	Filler Size 31 μm	Filler Size 164 μm
1	Quartz	SiO ₂	81	83
2	Zirconium Oxide	ZrO ₂	2	0
3	Magnetite	Fe ₂ O ₃	12	12
4	Anatase	TiO ₂	5	5

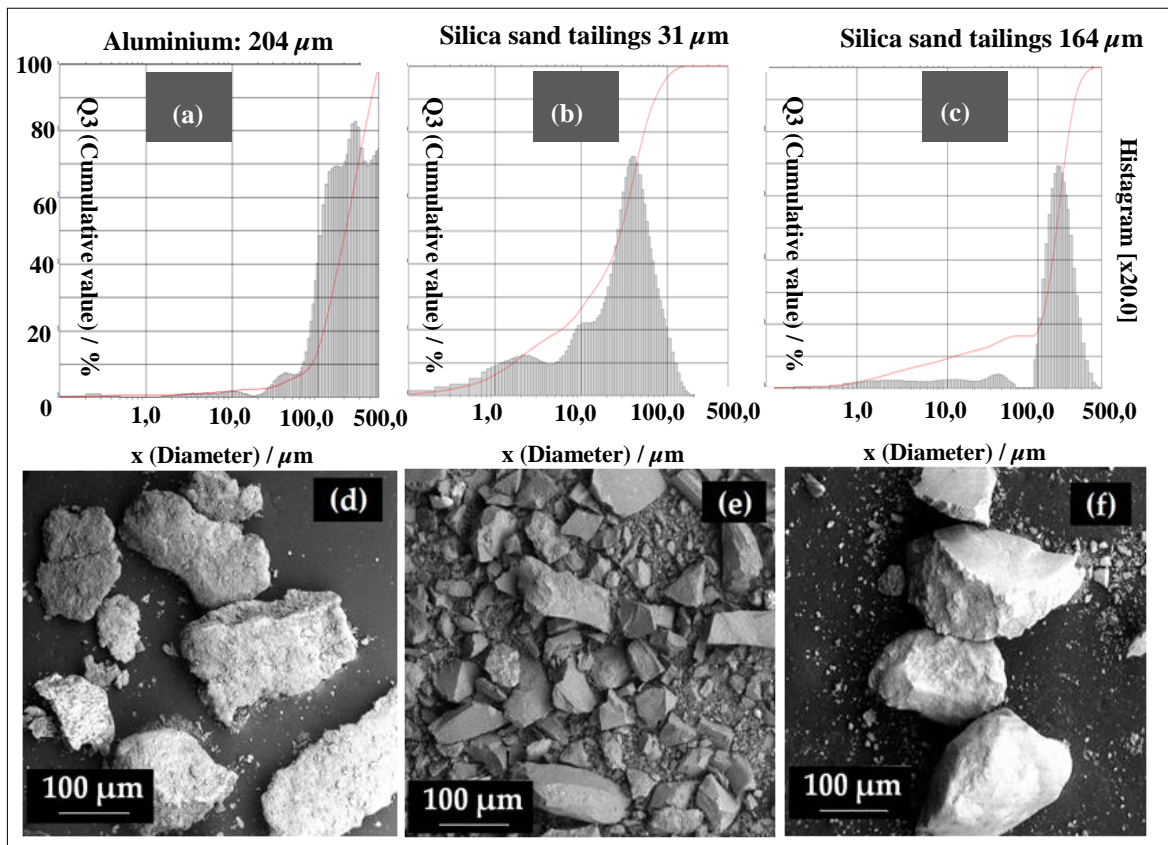


Figure 2. PSA Powder Measurement Charts and Phenom SEM Images of Powder Surface Morphology: (a) PSA, Al-ZnSiFeCuMg aluminium D50 = 204 μm , (b) PSA, silica tailings D50 = 31 μm , (c) PSA, silica tailings D50 = 164 μm , (d) SEM image, Al-ZnSiFeCuMg aluminium D50 = 204 μm , (e) SEM image, silica sand tailings D50 = 31 μm and (f) SEM image, silica sand tailings D50 = 164 μm

The filler powder material utilized silica sand that comes from tin mining leaching waste in Mentok in the Province of Bangka-Belitung Islands, which is called silica sand tailings. The size of silica sand tailings ranges from 50 - 60 mesh or 267 μm - 250 μm . These were processed by a ball mill to reduce the grain size, followed by sieving [44]. There are two classifications of grain size sieving that are used as fillers in the manufacture of the AMCs: 550-325 mesh (25 μm - 44 μm) and 120-70 mesh (125 μm - 210 μm). Next, silica tailings powder was measured using the PSA instrument and the PSA average size distribution was found to be D50: 31 μm \pm 4.49 and D50: 164 μm \pm 3.59. The results of PSA measurements are shown in Figure 2(b) and (c).

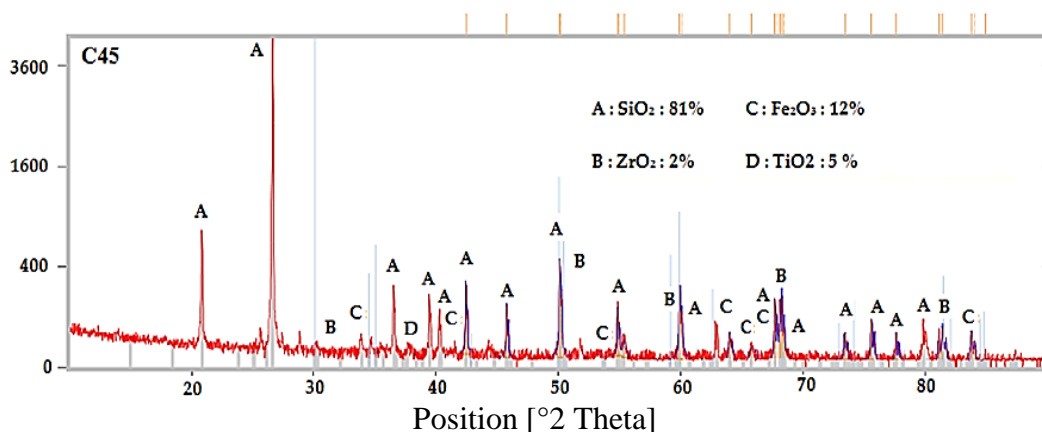


Figure 3. Graph of XRD test results for silica sand tailing powder D5=31 μm \pm 4.49

The aluminium alloy powder had a whitish-grey colour and tended to be flat and elongated in shape, but a small portion had a spherical shape [45, 46]. The aluminium powder was obtained after being machined by a lathe into chips and processed by a ball mill, as shown in Figure 2(d). Whereas the silica sand tailings tended to be brown, and after being processed by a ball mill, most were spherical and rounded, and some were angular and cubical [21, 47, 48], as shown in

Figure 2(e) and (f). The XRD silica sand tailings test results are shown in Table 2, and the graph is shown in Figure 3 for 31 μm and Figure 4 for 164 μm silica sand tailings.

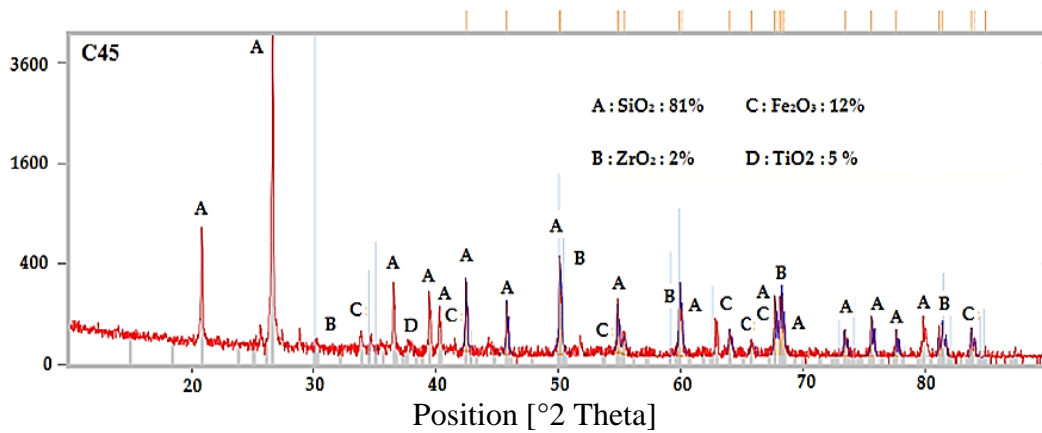


Figure 4. Graph of XRD test results for silica sand tailing powder D50 = 164 $\mu\text{m} \pm 3.59$

RESULTS AND DISCUSSION

Density and Porosity

The theoretical density of the Al-ZnSiFeCuMg aluminium alloy matrix was determined by referring to the results of chemical element composition testing using a laser spectrometer, as shown in Table 1. The calculations used Equation (1) to obtain the theoretical density value of Al-ZnSiFeCuMg aluminium alloy, which is 3,087 grams / cm³. Meanwhile, the theoretical density of the silica tailings filler material was determined by referring to the data from the XRD test in Table 2. The calculation of the theoretical density of filler powder with 31 μm grain size is 3.100 grams / cm³ and filler powder with 164 μm grain size is 3.040 grams / cm³. To determine the theoretical density values of the matrix and filler mixture, the percentage variable for the filler mass of AMCs, wt.% SiO₂, was applied, being 0%, 5%, 10%, 15%, 20%, 25%, and 30%. The hot-compaction density testing (ρ_{H-C}) and sintered density testing (ρ_S) of AMCs were carried out using Archimedes' principle.

The calculated theoretical density values and the density values from the above measurements were then combined and tabulated. Table 3 shows the theoretical density (ρ_T) values of AMCs with 31 μm filler and 164 μm filler. The theoretical density values of AMCs with 164 μm filler are relatively smaller than the theoretical density values of AMCs with 31 μm filler. Several factors cause these differences in values; first, the density of 164 μm filler powder is less than the matrix density, and the density of 31 μm filler powder is higher than the matrix density. Second, there are differences in the compounds contained in the 164 μm filler, which contains the ZrO₂ compound, while in the 31 μm filler, the ZrO₂ compound was not found, as shown in Table 2. Conversely, SiO₂ content with a low density increased from 81% to 83%.

Base on the data density values of Table 3, the calculation was then performed to determine the percentage value of the porosity of each AMCs used Equation (3); the result showed that AMCs specimens with a filler size of 31 μm had greater porosity values than AMCs specimens with a filler size of 164 μm . This condition is caused by the electrostatic energy of the powder which increases proportionately with a decrease in powder size, then produces some agglomeration and then forms several porous structures when the compaction process takes place, as shown in Figure 5. The porosity values of the produced AMCs specimens generally tended to decrease and then increase with increased filler wt.%. The AMCs specimen with a filler size of 164 μm with wt. 20% SiO₂, AMCs-31 μm -20% SiO₂, had the lowest porosity value, and the AMCs specimen with a filler size of 31 μm with wt. 30% SiO₂, AMCs-31 μm -30% SiO₂, had the highest porosity.

Table 3. Variations of the density of AMCs with 31 μm and 164 μm filler grain size

wt. %	31 μm filler grain size				164 μm filler grain size			
	Specimen Code	ρ_T	ρ_{H-C}	ρ_S	Specimen Code	ρ_T	ρ_{H-C}	ρ_S
		[gr/cm ³]				[gr/cm ³]		
0	AMCs-non-filler	3.087	2.401	2.563	AMCs-non-filler	3.087	2.401	2.563
5	AMCs-31 μm - 5% SiO ₂	3.088	2.306	2.433	AMCs-164 μm - 5% SiO ₂	3.085	2.344	2.554
10	AMCs-31 μm - 10% SiO ₂	3.088	2.260	2.381	AMCs-164 μm - 10% SiO ₂	3.082	2.307	2.506

15	AMCs-31 μm - 15% SiO_2	3.089	2.268	2.428	AMCs-164 μm - 15% SiO_2	3.080	2.330	2.535
20	AMCs-31 μm - 20% SiO_2	3.090	2.246	2.448	AMCs-164 μm - 20% SiO_2	3.078	2.345	2.571
25	AMCs-31 μm - 25% SiO_2	3.090	2.246	2.357	AMCs-164 μm - 25% SiO_2	3.075	2.290	2.460
30	AMCs-31 μm - 30% SiO_2	3.091	2.223	2.334	AMCs-164 μm - 30% SiO_2	3.073	2.292	2.379

The formation of high porosity in AMCs specimens occurs during the processes of hot-compaction and sintering, which are strongly influenced by hot-compaction pressure, sintering temperature, cooling time, and process environment. Also, this is influenced by several innate factors of powder materials, such as grain size distribution, grain shape, fluidity, agglomeration, lubrication effect, and others [21, 22]. During the process of AMCs specimen production, the surrounding air in the environment was not controlled, which resulted in a volume of trapped air when the surface area of the specimens underwent the cooling process. Shrinkage from the resulting semisolid had left voids in the grain boundary, which resulted in the formation of open pores on the surface and closed pores inside. This was also influenced by the agglomeration and segregation that occurred in AMCs with the smaller filler size (31 μm), as shown in Figure 7 (b, d, and f), where the powder clumping that occurred at the grain boundaries covered up small gaps when the cooling process took place.

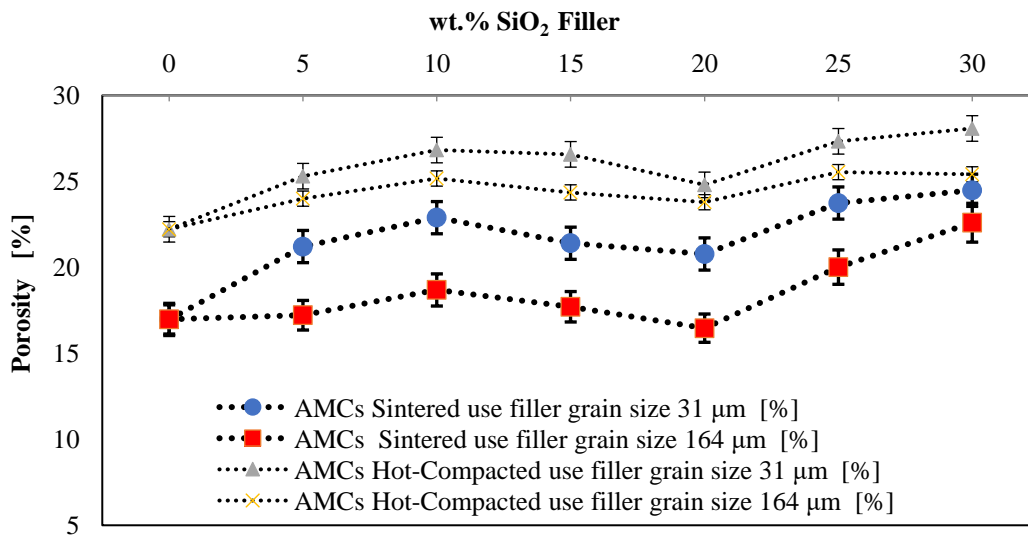


Figure 5. Graph of Porosity AMC uses filler grain size 31 μm versus 164 μm

Hardness

The AMCs specimen with non-filler and produced by the hot-compaction process showed a hardness value of 38.67 HRB. Figure 6 shows the chart comparing the hardness values of AMCs specimens using a filler powder of 31 μm and 164 μm sizes. The hardness values of AMCs with 164 μm filler size tended to increase with increased wt.% SiO_2 , but after exceeding 20% SiO_2 , the hardness values of the specimens decreased, up to 30% SiO_2 . The same trend occurred in the hardness values of AMCs with 31 μm filler size, the difference being that the decrease was after exceeding 15% SiO_2 . This condition shows that a greater percentage of filler leads to greater dispersion strengthening; however, if the percentage of filler continues to be increased above 15-20%, then the filler powder cannot evenly fill small gaps, because smaller grain sizes lead to greater agglomeration and segregation or poor homogenous. Besides, the capability of the matrix for wettability and as a binder for a given filler volume decreases with increased wt.% of filler. This results in the mechanical bond between the surface matrix and the filler becoming weaker, as shown in Figure 7.

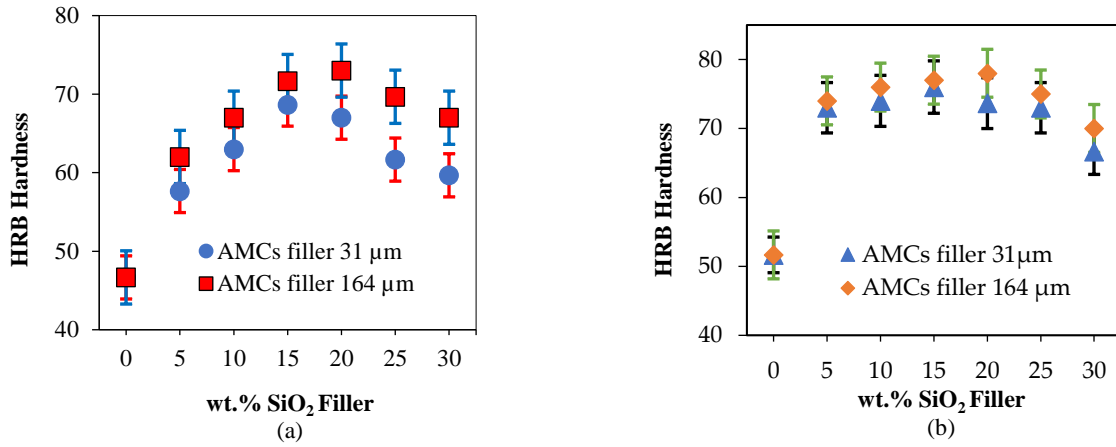


Figure 6. Hardness Graph of AMCs: (a) Hot-Compaction AMCs with 31 μm versus 164 μm fillers and (b) Sintered AMCs with 31 μm versus 164 μm fillers

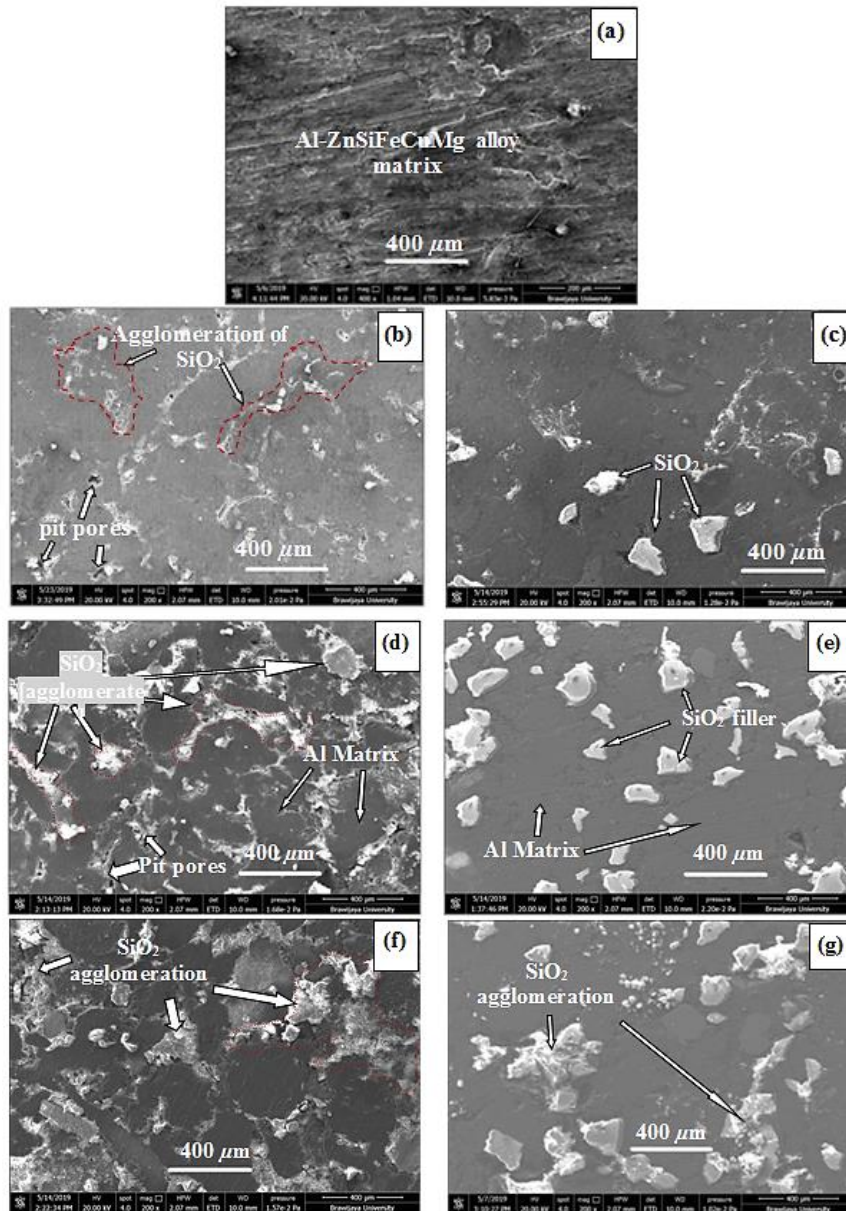


Figure 7. Secondary Electron (SE) SEM Images of AMCs Specimen Microstructures: (a) AMCs wt.0% SiO₂ (non-filler) (b) AMCs-31 μm -10% SiO₂, (c) AMCs-164 μm -10% SiO₂, (d) AMCs-31 μm-20% SiO₂, (e) AMCs-164 μm -20% SiO₂, (f) AMCs-31 μm -30% SiO₂ and (g) AMCs-164 μm -30% SiO₂

AMCs specimens with 164 μm filler showed higher hardness values than AMCs with 31 μm filler. In the process of powder metallurgy, this condition is mainly influenced by the agglomeration that occurs with a smaller filler size (31 μm) compared to agglomeration with a larger filler size (164 μm) as shown in the images in Figure 7(b, d, f). This agglomeration is caused by the electrostatic energy of the powder, increasing in proportion to the decrease in powder size. The spread of 164 μm filler in AMCs occurred more evenly compared to the 31 μm filler, which tends to agglomerate, as shown in Figure 7(c, e, g). The best filler spread occurred for the AMCs-164 μm -20% SiO_2 specimen, as in Figure 7(e). Therefore, the greatest hardness value occurred for that specimen, with a hardness value of 78 HRB. The value for AMCs with non-filler only reached 46.67 HRB. Thus, the addition of filler powder for the AMCs-164 μm -20% SiO_2 specimen was able to increase AMCs hardness by up to 67%. Whereas, the highest hardness value for AMCs with 31 μm filler powder reached 76 HRB or increased by 63%.

The problem of agglomeration that occurs in mixing powders of small sizes can be avoided through a mixing process that is performed better or more perfectly, for example mixing with the mechanical alloying method or mixing with chemical solutions to increase wettability, adhesiveness, and binding capacity [21, 22]. Consequently, this requires additional processes and costs.

Wear Rate

The data of the wear friction test is used to determine wear rate value by using Eq (4). The calculation results are shown in graph Figure 8. The lowest wear rate value was for the AMCs-164 μm -20% SiO_2 specimen. AMCs specimens from both the hot-compaction process and the sintering process showed higher wear rate values for AMCs with a filler size of 164 μm compared to AMCs with a filler size of 31 μm .

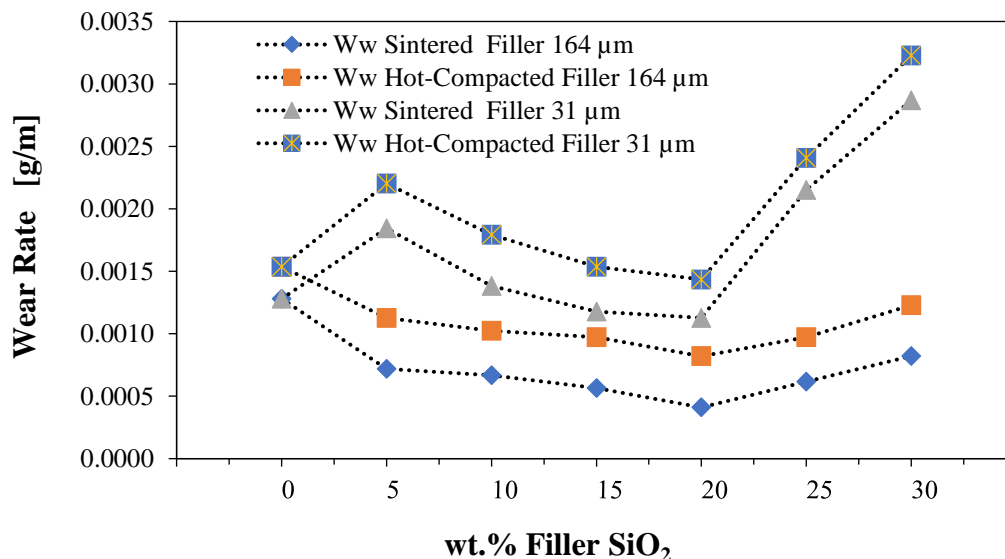


Figure 8. Wear rates of AMCs with 31 μm versus 164 μm fillers

Microstructure and Analysis

Microstructure analysis shown by Secondary Electron (SE) SEM images of Figure 9, supported confidence in the calculation of porosity (Table 3). SE SEM images of Figure 9(a) and (b) showed AMCs specimens' porosity without filler powder (low fillers). As well, SE SEM images of Figure 9(c) and (d) showed an increase in the number of pit pores, which are presented on the side of the enlarged image (on the 100 μm scale image). However, SE SEM images of Figure 9(e) and (f) showed the opposite condition, being a decrease in porosity, with a tendency for shallow-pore morphologies to appear, which are presented on the side of the enlarged image (on the 100 μm scale image). Finally, images of Figure 9(g) and (h) again showed an increase in porosity, even showing wide-pit pore morphologies, in which without an enlargement image, the pores are visible.

Figure 10 shows SE images from SEM photography of the imprints on several AMCs specimens as a reference for the analysis of the level and type of wear that occurred. SE images of Figure 10(a), (b) show the occurrence of plastic deformation and formation of deep groups, which indicate the occurrence of a mild-wear process through simultaneous adhesive wear and abrasive wear in AMCs specimens non-filler. The image of Figure 10(c) shows the chemical composition of elements found in the friction observation area, from SEM-EDS analysis results. The friction area of the matrix specimen was dominated by elements Al, O, Si, Cu, and Fe, and thus it may be possible that most of friction surface area contained the aluminium alloy matrix phase (Al-ZnSiFeCuMg), and a small amount of SiO_2 phase and Cu (FeO_2) phase impurities, as shown in Table 4.

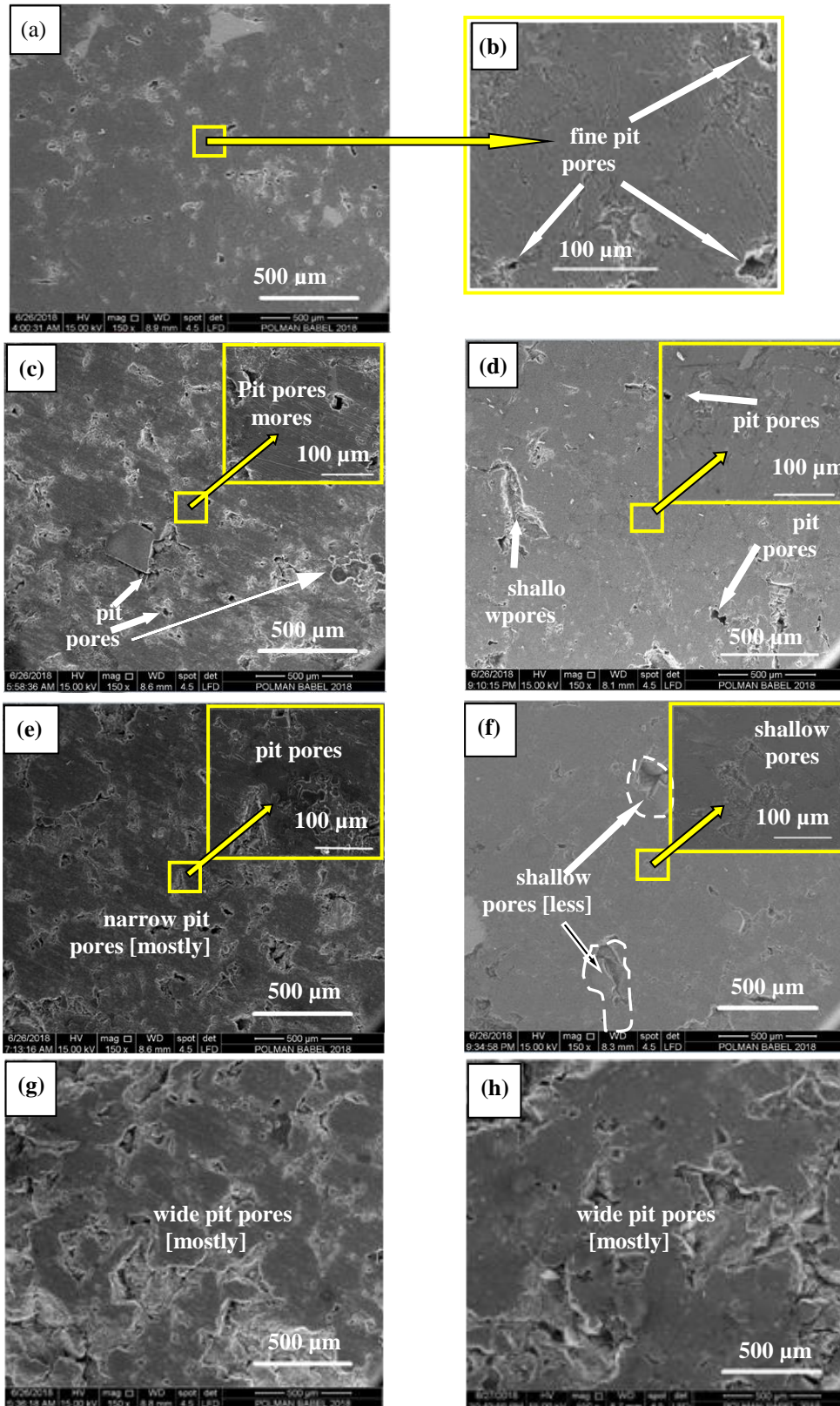


Figure 9. Secondary Electron (SE) SEM Images of AMCs Specimen Pores: (a, b) AMCwt.0% SiO₂ (non filler) (c) AMCs-31 μm -10% SiO₂, (d) AMCs-164 μm-10% SiO₂, (e) AMCs-31 μm -20% SiO₂, (f) AMCs-164 μm-20% SiO₂, (g) AMCs-31 μm -30% SiO₂ and (h) AMCs-164 μm-30% SiO₂

Figure 10(d), (e) shows the SE images of AMCs-31 μm -10% SiO₂ AMCs, where the friction that occurred resulted in plastic deformation, abrasive wear, and formation of shallow grooves, indicating mild-wear. Figure 10(f), (g) shows that for the AMC-164 μm -10% SiO₂ specimen, cracks and abrasion occurred, indicating or characterizing hard-wear. Next, Figure 10(h), (i) shows the hard-wear process that occurs in AMCs-31 μm-20% SiO₂ AMCs. Wear delamination

occurred in AMCs with wt.20%, especially in AMCs specimens with a filler size of $164\ \mu\text{m}$, as shown in SE images of Figure 10(j), (k) for the AMC- $164\ \mu\text{m}$ -10% SiO_2 specimen. The distribution of the SiO_2 powder dispersal, as shown in the SE image from Figure 7(e), affected the hard friction that occurred for the AMCs- $164\ \mu\text{m}$ -10% SiO_2 specimen, and thus it is the specimen with the highest wear resistance and the lowest wear rate. Meanwhile, SE images from Figure 10 images covers ; 10 (l), (m), (n), and (o) show the specimens with the highest wt.% of SiO_2 (30%), where severe abrasive wear occurred, evidenced by the high amount of debris wear found for these specimens.

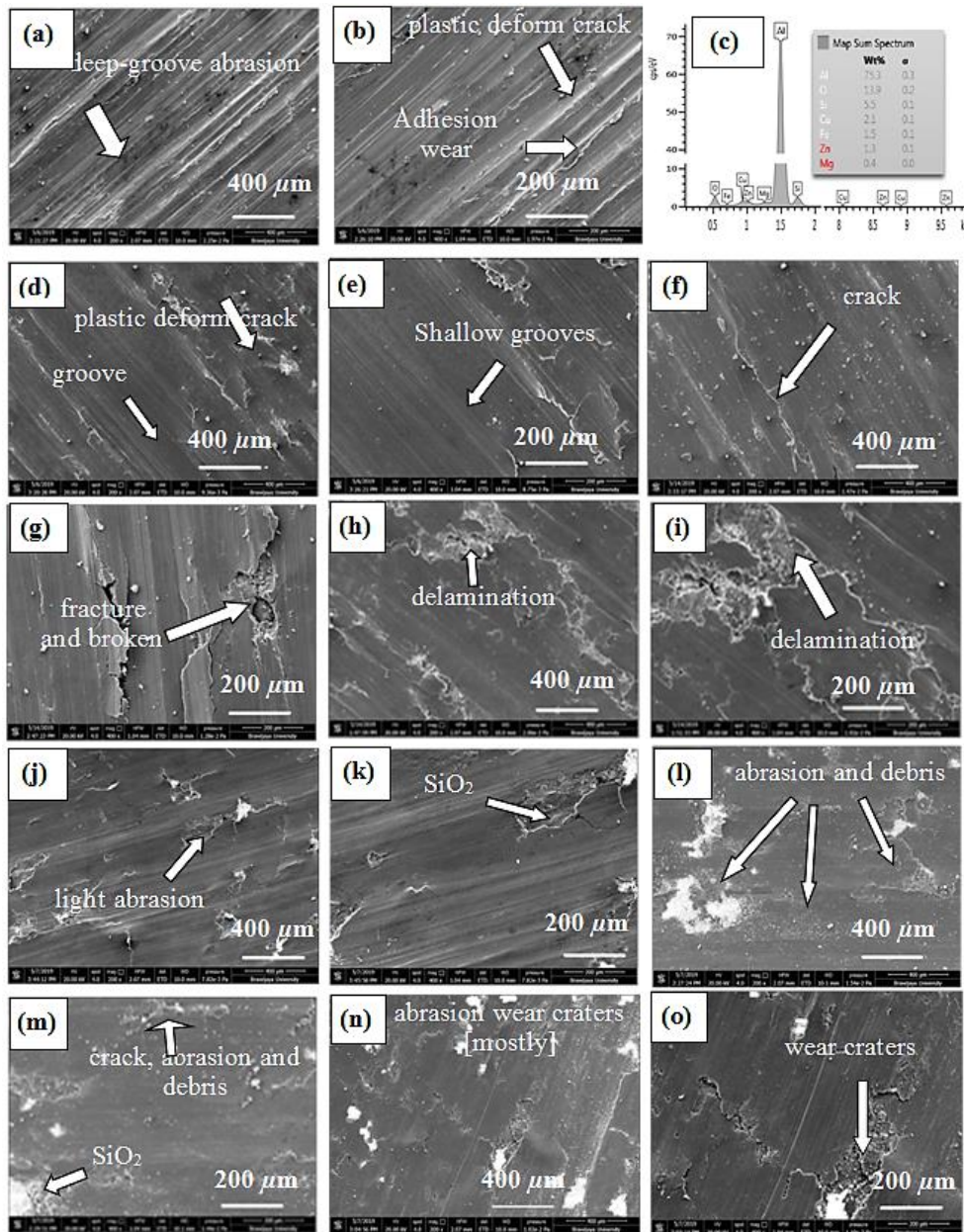


Figure 10. Secondary Electron (SE) SEM Images of AMCs Specimen Wear: (a) and (b) AMCs non-filler, (c). EDS element of AMCs non-filler, (d) and (e) AMCs- $31\ \mu\text{m}$ -10% SiO_2 , (f) and (g) AMCs- $164\ \mu\text{m}$ -10% SiO_2 , (h) and (i) AMCs- $31\ \mu\text{m}$ -20% SiO_2 , (j) and (k) AMCs- $164\ \mu\text{m}$ -20% SiO_2 , (l) and (m) AMCs- $31\ \mu\text{m}$ -30% SiO_2 , (n) and (o) AMCs- $164\ \mu\text{m}$ -30% SiO_2

Table 4 shows the results of SEM-EDS observations regarding the composition of chemical elements found on the surface of the specimen friction plane. Seven main elements appeared for each examined AMCs specimen. However, three dominant elements were always found for each specimen, being aluminium (Al), oxygen (O), and silicon (Si), with the total composition of the three elements averaging above 97.5%. Therefore, from the results of SEM-EDS observations, it can be assumed that the phases contained for each specimen are a matrix of Al, O, and SiO_2 .

Detailed analysis of AMCs specimens with filler sizes of $164\ \mu\text{m}$ and $31\ \mu\text{m}$ found that there were significant differences regarding the levels of SiO_2 contained in the two groups of specimens. The Si content of AMCs- $31\ \mu\text{m}$ -20% SiO_2 was 8.4 % less than the Si content of the AMCs- $164\ \mu\text{m}$ -20% SiO_2 specimen, which was 12.1%, although the research design instituted the addition of SiO_2 filler of the same wt.% (wt.20%). The condition also occurred for the AMCs- $31\ \mu\text{m}$ -30% SiO_2 specimen, which had a smaller Si level of 8.4% compared to the AMCs- $164\ \mu\text{m}$ -30% SiO_2

specimen, which was 12.7%, even though the added SiO₂ fillers were of the same wt.%. So, the specimens with 31 μm filler, agglomeration and segregation has a high chance of occurring, as shown in Figure 7(d, f), which results in a weaker mechanical bond between the surface of the matrix and the surface of the filler, and consequently greater wear and SiO₂ erosion as evidenced by the wear test, in comparison to AMCs with 164 μm filler. Therefore, AMCs with the addition of SiO₂ filler of 164 μm powder size had a lesser wear rate or greater wear resistance than AMCs with the 31 μm filler, being 0.00041 g/m and 0.00113 g/m respectively.

Table 4. List of chemical compositions of each specimen at the friction area test by SEM-EDS analysis

Element Specimen	Al	O	Si	Cu	Fe	Zn	Ti	Other	Possible phase matrix
	Wt (%)								
AMCs non- filler	75.3	13.9	5.5	2.1	1.5	1.3	-	0.4	Al, SiO ₂ , Cu(FeO ₂)
AMCs-31μm- 10% SiO ₂	64.6	20.7	8.6	2.2	2.1	1.7	-	0.1	Al, SiO ₂ , Cu (FeO ₂),ZnO
AMCs-164 μm -10% SiO ₂	64.2	21.2	8.3	2.3	2.0	1.6	0.4	-	Al, SiO ₂ ,Cu (FeO ₂),TiO
AMCs-31μm - 20% SiO ₂	40.3	35.5	8.4	1.7	2.4	1.2	0.1	0.2	Al,SiO ₂ , Cu (FeO ₂),TiO
AMCs-164 μm -20% SiO ₂	50.8	30.9	12.1	1.8	2.1	1.2	0.9	0.2	Al, SiO ₂ , Cu (FeO ₂),TiO
AMCs-31 μm - 30% SiO ₂	38.7	41.8	8.4	1.0	1.8	1.5	0.2	0.5	Al, SiO ₂ , Cu (FeO ₂),TiO
AMCs-164 μm -30% SiO ₂	40.8	41.6	12.7	1.5	2.3	0.5	0.6	0.5	Al, SiO ₂ , Cu (FeO ₂),TiO

CONCLUSIONS

The research on the production of AMCs using a matrix of Al-ZnSiFeCuMg aluminium alloy reinforced with silica sand tailings filler, using the powder metallurgy method and involving several material characterizations, had been successfully carried out and resulted in the following conclusions:

- 1) Testing of the chemical composition of recycled Al-ZnSiFeCuMg aluminium alloy using laser Spectro and EDS indicated several element impurities such as Ca, Zr, Mg, Ti, and others up to a maximum impurity percentage of 0.5%. However, this aluminium alloy can function as the best matrix and binder for adding silica sand tailing fillers with a percentage of weight 20%, compared to variations in other weight percentages of fillers (5%-10%-15%-25%-30%).
- 2) Silica sand tailings from tin mining waste in Bangka Belitung, Indonesia, has SiO₂ levels that exceed 80%. The silica tailings powder can be used directly as a filler in the manufacture of AMCs without having to undergo the leaching process first, which requires a very high cost.
- 3) Results of observations using SEM images showed that the use of silica tailings filler of 31 μm grain size in the manufacture of AMCs tended to lead to high agglomeration and segregation compared to silica tailings filler of 164 μm grain size. This agglomeration resulted in relatively high porosity of AMCs, between 16% - 25%.
- 4) The mechanical properties of AMCs with silica tailings filler of 164 μm grain size were better than AMCs with silica tailings filler of 31 μm grain size. The addition of silica tailings filler of 164 μm grain size up to wt.20% to the Al-ZnSiFeCuMg aluminium alloy matrix was able to increase the hardness of AMCs by 67%, from 46.67 HRB in AMCs non-filler to 78 HRB, with a wear rate of 0.00041 g/m. Meanwhile, the addition of silica tailings filler of 31 μm grain size up to wt.20% to the Al-ZnSiFeCuMg aluminium alloy matrix could increase the hardness of AMCs by 63%, from 46.67 HRB to 76 HRB, with a wear rate of 0.00113 g/m.
- 5) The wear test result using the pin-on-disc method, then characterized using the SE image SEM-EDS analysis has helped to clarify the phenomenon of severe-mild wear rate that occurs. The smallest percentage of silica filler weight (wt.5% SiO₂) showed the occurrence of severe adhesion wear because the matrix material is mild and ductile, while the largest percentage of silica filler weight (wt.30% SiO₂) showed the occurrence of severe abrasion wear due to the influence of filler clumping and brittleness.

ACKNOWLEDGEMENTS

The Scholarship supports this work for Leading Indonesian Lecturers – National Education (BUDI-DN) and the Educational Fund Management Institution (LPDP) under grant number PRJ-6506/LPDP.3/2016. As well as grants and collaboration with Pt. Timah.tbk., Pangkal Pinang, Indonesia.

REFERENCES

- [1] J. Eliasson and R. Sandström, “Applications of Aluminium Matrix Composites,” *Key Eng. Mater.*, vol. 104–107, pp. 3–36, Mar. 2009, doi: 10.4028/www.scientific.net/kem.104-107.3.
- [2] C. C. Nwobi-Okoye and B. Q. Ochieze, “Age hardening process modeling and optimization of aluminum alloy A356/Cow horn particulate composite for brake drum application using RSM, ANN and simulated annealing,” *Def. Technol.*, vol. 14, no. 4, pp. 336–345, 2018, doi: 10.1016/j.dt.2018.04.001.
- [3] A. . Adebisi, M. . Maleque, and M. . Rahman, “Metal matrix composite brake rotor : historical development and product life cycle analysis,” *Int. J. Automot. Mech. Eng.*, vol. 4, no. July-Desember, pp. 471–480, 2011, doi: 10.15282/ijame.4.2011.8.0038.
- [4] P. Garg, A. Jamwal, D. Kumar, K. K. Sadasivuni, C. M. Hussain, and P. Gupta, “Advance research progresses in aluminium matrixcomposites: Manufacturing & applications,” *J. Mater. Res. Technol.*, vol. 8, no. 5, pp. 4924–4939, 2019, doi: 10.1016/j.jmrt.2019.06.028.
- [5] A. Kurt and M. Boz, “Wear behaviour of organic asbestos based and bronze based powder metal brake linings,” *Mater. Des.*, vol. 26, no. 8, pp. 717–721, 2005, doi: 10.1016/j.matdes.2004.09.006.
- [6] V. S. Aigbodion, U. Akadike, S. B. Hassan, F. Asuke, and J. O. Agunsoye, “Development of asbestos - free brake pad using bagasse,” *Tribol. Ind.*, vol. 32, no. 1, pp. 12–18, 2010, doi: http://www.tribology.rs/journals/2010/2010-1/2.
- [7] S. Furuya, O. Chimed-Ochir, K. Takahashi, A. David, and J. Takala, “Global asbestos disaster,” *Int. J. Environ. Res. Public Health*, vol. 15, no. 5, 2018, doi: 10.3390/ijerph15051000.
- [8] H. Ghandvar, M. H. Idris, N. Ahmad, and N. Moslemi, “Microstructure development, mechanical and tribological properties of a semisolid A356/xSiCp composite,” *J. Appl. Res. Technol.*, vol. 15, no. 6, pp. 533–544, 2017, doi: 10.1016/j.jart.2017.06.002.
- [9] A. A. Agbeleeye, D. E. Esezobor, S. A. Balogun, J. O. Agunsoye, J. Solis, and A. Neville, “Tribological properties of aluminium-clay composites for brake disc rotor applications,” *J. King Saud Univ. - Sci.*, vol. xxx, pp. xxx–xxx, 2017, doi: 10.1016/j.jksus.2017.09.002.
- [10] A. P. S. V. R. Subrahmanyam, J. Madhukiran, G. Naresh, and S. Madhusudhan, “Fabrication and characterization of Al356.2, rice husk ash and fly ash reinforced hybrid metal matrix composite,” *Int. J. Adv. Sci. Technol.*, vol. 94, pp. 49–56, 2016, doi: 10.14257/ijast.2016.94.05.
- [11] C. U. Atuanya, D. I. Ekweghiariri, and C. M. Obele, “Experimental study on the microstructural and anti-corrosion behaviour of Co-deposition Ni–Co–SiO2 composite coating on mild steel,” *Def. Technol.*, vol. 14, no. 1, pp. 64–69, 2018, doi: 10.1016/j.dt.2017.10.001.
- [12] E. Velasco and J. Nino, “Recycling of aluminium scrap for secondary Al-Si alloys,” *Waste Manag. Res.*, vol. 29, no. 7, pp. 686–693, 2011, doi: 10.1177/0734242X10381413.
- [13] EAFA, “Environmental Profile Report 2018 on Life-Cycle inventory data for aluminium production and transformation processes in Europe,” in *European Aluminium*, February 2., no. The Aluminium Effect, Avenue de Tervueren 168 B-1150 Brussels, Belgium: European Aluminium, 2018.
- [14] S. Liu, X. Li, and M. Wang, “Analysis of aluminum resource supply structure and guarantee degree in China based on sustainable perspective,” *Sustain.*, vol. 8, no. 12, pp. 1–17, 2016, doi: 10.3390/su8121335.
- [15] Sukarman and R. A. Gani, “Ex-mining Land in Bangka and Belitung Islands, Indonesia and Their Suitability for Agricultural Commodities,” *J. Tanah dan Iklim*, vol. 41, no. 2, pp. 101–112, 2017, doi: 10.2017/jti.v41i2.7176.
- [16] N. R. Setiati, “The Potential Use of Silica Sand as Nanomaterials for Mortar,” in *AIP Conference Proceedings 1903*, 2017, vol. 050010, doi: 10.1063/1.5011549.
- [17] L. P. Santi, D. Mulyanto, and D. H. Goenadi, “Double Acid-Base Extraction of Silicic Acid from Quartz Sand,” *J. Miner. Mater. Charact. Eng.*, vol. 05, no. 06, pp. 362–373, 2017, doi: 10.4236/jmmce.2017.56030.
- [18] A. Wahyudi, A. Dessy, and Sariman, “Preparation of Nano Silica from Silica Sand Through Alkali Fusion,” *Indones. Min. J.*, vol. 16, no. october 2013, pp. 149–153, 2013, doi: 10.30556/imj.Vol16.No3.2013.383.
- [19] M. Xing, Z. Fu, Y. Wang, J. Wang, and Z. Zhang, “Lead recovery and high silica glass powder synthesis from waste CRT funnel glasses through carbon thermal reduction enhanced glass phase separation process,” *J. Hazard. Mater.*, vol. 322, pp. 479–487, 2017, doi: 10.1016/j.jhazmat.2016.10.012.
- [20] A. Fuad, N. Mufti, M. Diantoro, Subakti, and S. Septa Kurniawati, “Synthesis and characterization of highly purified nanosilica from pyrophyllite ores,” in *AIP Conference Proceedings*, 2016, vol. 1719, doi: 10.1063/1.4943715.
- [21] S. H. Huo, M. Qian, G. B. Schaffer, and E. Crossin, “Aluminium powder metallurgy,” *Fundam. Alum. Metall. Woodhead Publ. Ltd.*, 2011, doi: 10.1533/9780857090256.3.655.
- [22] C. Suryanarayana, “Mechanical alloying and milling,” *Prog. Mater. Sci.*, vol. 46, pp. 1–184, 2001, doi: PII: S0079-6425(99)00010-9.

- [23] M. Sherif El-Eskandarany, *Mechanical Alloying, Nanotechnology, Material Sciences and Powder Metallurgy*, Second Edi., vol. 39, no. 8. Kuwait: Kuwait Institute for Scientific Research, 1987.
- [24] K. R. Kumar, K. M. Mohanasundaram, G. Arumaikkannu, and R. Subramanian, "Effect of particle size on mechanical properties and tribological behaviour of aluminium/fly ash composites," *Sci. Eng. Compos. Mater.*, vol. 19, no. 3, pp. 247–253, 2012, doi: 10.1515/secm-2011-0139.
- [25] P. M. Gopal, K. Soorya Prakash, S. Nagaraja, and N. Kishore Aravinth, "Effect of weight fraction and particle size of CRT glass on the tribological behaviour of Mg-CRT-BN hybrid composites," *Tribol. Int.*, vol. 116, pp. 338–350, 2017, doi: 10.1016/j.triboint.2017.07.025.
- [26] S. K. Jo, W. J. Lee, Y. H. Park, and I. M. Park, "Effect of SiC particle size on wear properties of Al₂O₃/SiC/Mg hybrid metal matrix composites," *Tribol. Lett.*, vol. 45, no. 1, pp. 101–107, 2012, doi: 10.1007/s11249-011-9866-7.
- [27] J. K. Chen, T. P. Tang, S. F. Chan, and S. H. Chang, "Effects of particle size on mechanical properties of a TiC containing tool steel by hot isostatic press," *Mater. Trans.*, vol. 49, no. 3, pp. 624–628, 2008, doi: 10.2320/matertrans.MER2007262.
- [28] J. Liu *et al.*, "Effect of powder metallurgy synthesis parameters for pure aluminium on resultant mechanical properties," *Int. J. Mater. Form.*, vol. 12, no. 1, pp. 79–87, 2019, doi: 10.1007/s12289-018-1408-5.
- [29] A. Chaubey, P. Konda Gokuldoss, Z. Wang, S. Scudino, N. Mukhopadhyay, and J. Eckert, "Effect of Particle Size on Microstructure and Mechanical Properties of Al-Based Composite Reinforced with 10 Vol.% Mechanically Alloyed Mg-7.4%Al Particles," *Technologies*, vol. 4, no. 4, p. 37, Nov. 2016, doi: 10.3390/technologies4040037.
- [30] Y. C. Huang, C. H. Su, S. K. Wu, and C. Lin, "A study on the hall-petch relationship and grain growth kinetics in FCC-structured high/medium entropy alloys," *Entropy*, vol. 21, no. 3, pp. 1–13, 2019, doi: 10.3390/e21030297.
- [31] S. A. Sajjadi, H. R. Ezatpour, and H. Beygi, "Microstructure and mechanical properties of Al-Al₂O₃ micro and nano composites fabricated by stir casting," *Mater. Sci. Eng. A*, vol. 528, no. 29–30, pp. 8765–8771, 2011, doi: 10.1016/j.msea.2011.08.052.
- [32] M. A. Maleque, S. Dyuti, and M. M. Rahman, "Material selection method in design of automotive brake disc," in *Proceedings of the World Congress on Engineering 2010 Vol III WCE 2010, June 30 - July 2, 2010, London, U.K.*, 2010, vol. III, pp. 2322–2326.
- [33] H. L. Rizkalla and A. Abdulwahed, "Some mechanical properties of metal-nonmetal Al-SiO₂ particulate composites," *J. Mater. Process. Technol.*, vol. 56, pp. 398–403, 1996, doi: org/10.1016/0924-0136(96)85107-7.
- [34] Zuhailawati H., P. Samayamutthirian, and Mohd Haizu C.H., "Fabrication of low cost of aluminium matrix composite reinforced with silica sand," *J. Phys. Sci.*, vol. 18, no. 1, pp. 47–55, 2007, [Online]. Available: [http://www.usm.my/jps/18-1-07/Article 18-1-5.pdf](http://www.usm.my/jps/18-1-07/Article%2018-1-5.pdf).
- [35] S. Mohan, G. Gautam, N. Kumar, R. K. Gautam, A. Mohan, and A. K. Jaiswal, "Dry sliding wear behavior of Al-SiO₂ composites," *Compos. Interfaces*, vol. 23, no. 6, pp. 493–502, 2016, doi: 10.1080/09276440.2016.1149363.
- [36] N. K. Yusuf, M. A. Lajis, and A. Ahmad, "Hot press as a sustainable direct recycling technique of aluminium: Mechanical properties and surface integrity," *Materials (Basel)*, vol. 10, no. 8, 2017, doi: 10.3390/ma10080902.
- [37] I. A. Wahyudie, R. Soenoko, W. Suprpto, and Y. S. Irawan, "Optimizing warm compaction parameters on the porosity and hardness of Bronze/Tin ore waste composites," in *IOP Conference Series: Materials Science and Engineering*, 2019, vol. 494, no. 1, pp. 0–12, doi: 10.1088/1757-899X/494/1/012101.
- [38] W. Suprpto, "Processed of Sand Ore Iron Oxide Ferro Low as Raw Steel in Reveberatory Furnace," in *Proceedings of the 2015 International Conference on Advanced Manufacturing and Industrial Application*, 2015, no. Advances in Engineering Research, pp. 26–30, doi: 10.2991/icamia-15.2015.7.
- [39] ASTM International, "Standard Test Methods for Density of Compacted or Sintered Powder Metallurgy (PM) Products Using Archimedes' Principle," *Asm B962-13*, vol. i, pp. 1–7, 2013, doi: 10.1520/B0962-13.2.
- [40] M. Chegini, M. H. Shaeri, R. Taghiabadi, S. Chegini, and F. Djavanroodi, "The Correlation of Microstructure and Mechanical Properties of In-Situ Al-Mg₂Si Cast Composite Processed by Equal Channel Angular Pressing," *Materials (Basel)*, vol. 12, no. 9, pp. 1–12, 2019, doi: 10.3390/ma12091553.
- [41] M. Nagaral, V. Auradi, S. A. Kori, and V. Hiremath, "Investigations on mechanical and wear behavior of nano Al₂O₃ particulates reinforced AA7475 alloy composites," *J. Chem. Inf. Model.*, vol. 53, no. 9, pp. 1689–1699, 2013, doi: 110.15282/jmes.13.1.2019.19.0389.
- [42] I. A. Wahyudie, R. Soenoko, W. Suprpto, and Y. S. Irawan, "Enhancing hardness and wear resistance of ZrSiO₄-SnO₂ / Cu₁₀Sn composite produced by warm compaction and sintering," *metalurgija*, 2020.
- [43] M. . Maleque, M. Radhi, and M. . Rahman, "Wear study of Mg-SiCp reinforcement aluminium metal matrix composite," *J. Mech. Eng. Sci.*, vol. 10, no. 1, pp. 1758–1764, 2016, doi: org/10.15282/jmes.10.1.2016.1.0169 Wear.
- [44] Sukanto, R. Soenoko, W. Suprpto, and Y. S. Irawan, "Parameter Optimization of Ball Milling Process for Silica Sand Tailing," *IOP Conf. Ser. Mater. Sci. Eng.*, vol. 494, no. 1, 2019, doi: 10.1088/1757-899X/494/1/012073.
- [45] M. Skalon, M. Hebda, R. Buzolin, G. Pottlacher, S. Mitsche, and C. Sommitsch, "Preparation method of spherical and monocrystalline aluminum powder," *Metals (Basel)*, vol. 9, no. 3, pp. 1–9, 2019, doi: 10.3390/met9030375.
- [46] S. Lucas, M. T. Tognonvi, J. L. Gelet, J. Soro, and S. Rossignol, "Interactions between silica sand and sodium silicate solution during consolidation process," *J. Non. Cryst. Solids*, vol. 357, no. 4, pp. 1310–1318, 2011, doi: 10.1016/j.jnoncrsol.2010.12.016.

- [47] R. Milke, "Geomaterials in the manuscript archive: the composition of writing sands and the regional distribution of writing-sand types in SW-Germany and northern Switzerland, 14th to 19th century," *Eur. J. Mineral.*, vol. 24, no. 4, pp. 759–770, 2012, doi: 10.1127/0935-1221/2012/0024-2207.
- [48] F. N. Ahmad, M. Jaafar, S. Palaniandy, and K. A. M. Azizli, "Effect of particle shape of silica mineral on the properties of epoxy composites," *Compos. Sci. Technol.*, vol. 68, no. 2, pp. 346–353, 2008, doi: 10.1016/j.compscitech.2007.07.015.